HHS Public Access

Author manuscript

J Invest Dermatol. Author manuscript; available in PMC 2015 November 01.

Published in final edited form as:

J Invest Dermatol. 2015 May ; 135(5): 1405–1414. doi:10.1038/jid.2014.411.

Mechanisms of Chemical Cooperative Carcinogenesis by Epidermal Langerhans Cells

Julia M. Lewis[1], **Christina D. Bürgler**[1], **Juliet A. Fraser**[1], **Haihui Liao**[1], **Kseniya Golubets**[1], **Cynthia L. Kucher**[2], **Peter Y. Zhao**[1], **Renata B. Filler**[1], **Robert E. Tigelaar**[1], and **Michael Girardi**[1]

[1]Department of Dermatology, Yale School of Medicine, New Haven, Connecticut, USA

[2]Greenwich Hospital, Greenwich, Connecticut, USA

Abstract

Cutaneous squamous cell carcinoma (SCC) is the most prevalent invasive malignancy with metastatic potential. The epidermis is exposed to a variety of environmental DNA-damaging chemicals, principal among which are polyaromatic hydrocarbons (PAH) ubiquitous in the environment, tobacco smoke, and broiled meats. Langerhans cells (LC) comprise a network of dendritic cells situated adjacent to basal, suprabasal, and follicular infundibular keratinocytes that when mutated can give rise to SCC, and LC-intact mice are markedly more susceptible than LC-deficient mice to chemical carcinogenesis provoked by initiation with the model PAH, 7,12-dimethylbenz[*a*]anthracene (DMBA). LC rapidly internalize and depot DMBA as numerous membrane-independent cytoplasmic foci. Repopulation of LC-deficient mice using fetal liver LC-precursors restores DMBA-induced tumor susceptibility. LC expression of p450 enzyme CYP1B1 is required for maximal rapid induction of DNA-damage within adjacent keratinocytes and their efficient neoplastic transformation; however, effects of tumor progression also attributable to the presence of LC were revealed as CYP1B1-independent. Thus, LC make multifaceted contributions to cutaneous carcinogenesis, including via the handling and metabolism of chemical mutagens. Such findings suggest a cooperative carcinogenesis role for myeloid-derived cells resident within cancer susceptible epithelial tissues principally by influencing early events in malignant transformation.

Introduction

The skin and other epithelial tissues are continually exposed to environmental chemicals and toxins, including those with carcinogenic potential. Mutagenic polyaromatic hydrocarbons (PAHs), generated largely as a result of industrial combustion exhaust and wastewater treatment discharges, have become prevalent in the atmosphere, soil, and ground water.

Address correspondence to: Michael Girardi, MD, Yale University School of Medicine, 333 Cedar Street, HRT 604D, New Haven, CT 06520-8059, United States, michael.girardi@yale.edu; Tel: 203-785-4092, Fax: 203-785-7637.

Conflict of Interest

The authors state no conflict of interest.

Automobile emissions, processed asphalt, coal burning, grilled or charred meats, and tobacco smoke also all contribute substantially to human PAH exposure. Furthermore, a variety of cosmetics and shampoos are made with coal tar and therefore may contain PAHs. As lipophilic compounds, PAHs are readily absorbed by cells; thus, PAH levels within plants and animals may be much higher than the PAH levels detected in their environments (ATSDR, 2011).

Skin exposure to PAHs may occur by direct contact, as well as via distribution to the skin after systemic absorption. People who smoke tobacco, for example, are exposed to high levels of the PAH benz[*a*]anthracene (Werley *et al.*, 2008) and show a >50% increased risk of developing SCC (Leonardi-Bee *et al.*, 2012). Mutagenic PAHs form stable, bulky covalent DNA-PAH adducts that lead to double-stranded (ds)DNA breaks and nucleic base mismatch reads. The cellular handling and metabolism of PAHs are therefore fundamental to understanding early events in chemical carcinogenesis. Most prior studies, however, have focused on the target epithelial cells of transformation, largely ignoring the other locally resident cells that may have substantial influence on these events.

Within the epidermis, a network of dendritic Langerhans cells (LC) extend to contact the vast majority of basal, suprabasal, and infundibular keratinocytes, in which tumor suppressor gene (e.g. p53) and oncogene (e.g. Ras) mutations may precipitate squamous cell carcinomas (SCC). Recently, we demonstrated that LC-deficient [huLangerin-DTA transgenic; DTA (Kaplan *et al.*, 2005)] mice are strikingly resistant to two-stage chemical carcinogenesis, and to *Hras* mutagenesis by DMBA (Modi *et al.*, 2012), despite the fact that the keratinocytes of such mice contain all the requisite enzymes for metabolism of DMBA. The abrogation of the requirement of LC for keratinocyte genotoxicity and tumor induction after topical application of the 3,4-diol DMBA metabolite implicated preferential metabolism of DMBA by LC to reactive intermediates, over detoxification. Consistent with this, murine LC were found to express cytochrome p450 enzyme CYP1B1, but not CYP1A1, and human LC express markedly higher levels of CYP1B1 than CYP1A1. Thus, we hypothesized that the high ratio of CYP1B1:CYP1A1 within LC biased metabolism of DMBA to mutagenic metabolites, inducing DNA-damage and provoking carcinogenesis in adjacent keratinocytes that themselves expressed high levels of both p450 enzymes, but in the inverse ratio (CYP1A1 > CYP1B1).

To further investigate the mechanisms by which LC facilitate chemical carcinogenesis, we herein studied the kinetics of LC handling of DMBA, and demonstrate that LC rapidly internalize and depot DMBA as numerous membrane-independent cytoplasmic foci that are excluded from LC nuclei. We developed a strategy for the repopulation of LC-deficient mice using fetal liver LC-precursors, and reestablished DMBA-induced tumor susceptibility, proportionate to levels of LC reconstitution. By neonatal repopulation of LC-deficient mice with fetal liver LC-precursors isolated from CYP1B1-deficient donors, we reveal that LC expression of CYP1B1 is required for maximal rapid induction of DNA-damage within adjacent keratinocytes, and as well as for their efficient neoplastic transformation. Nonetheless, LC also show the capacity to mediate pro-carcinogenic effects independently of CYP1B1. For example, consistent with a role for LC in increasing the bioavailability of mutagen independently of metabolism, mice repopulated with LC from CYP1B1−/− donors

are more susceptible to DMBA-induced DNA-damage than LC-deficient mice. In addition, effects on tumor progression attributable to the presence of LC were revealed as CYP1B1-independent. Thus, LC make multifaceted contributions to cutaneous carcinogenesis via their handling and metabolism of chemical mutagens, as well as their potentiation of tumor progression.

Results and Discussion

LC internalize DMBA and facilitate cutaneous carcinogenesis

Keratinocytes possess all the enzymatic requirements to metabolize DMBA to mutagenic forms; yet, application of DMBA followed by weekly promotion with the phorbol ester TPA much more readily facilitates tumor outgrowth in the presence of LC (Figure 1a). These data are consistent with mechanisms where LC enhance DMBA mutagenesis within adjacent epidermal stem cells. Moreover, 24 hours after topical cutaneous exposure to DMBA, we observed LC mRNA expression, surface protein and morphologic changes indicative of aryl hydrocarbon receptor (AhR)-mediated activation. In addition to our previous observation of increased CYP1B1 expression (Modi *et al.*, 2012) LC cell line XS106 also displayed mRNA levels increased for CD80 and CD207, and decreased for TLR4 (Figure 1b). As well, 24 hours after percutaneous application of DMBA, isolated LC displayed increased CD86 surface protein (Figure 1c) and, *in vivo*, converted from a dendritic to a more rounded morphology (Figure 1d,e). These changes are all consistent with that previously reported for AhR xenobiotic response element activation in myeloid-derived cells (Ilchmann *et al.*, 2012; Simones and Shepherd, 2011). Thus, we sought to better understand the characteristics of LC internalization of DMBA, and monitored XS106, as well as isolated murine epidermal LC, by time-lapse two-photon microscopy after *in vitro* exposure to DMBA. The multi-ringed structures of PAHs provide predictable spectral fluorescence properties, and DMBA fluoresces in the 440nm wavelength range upon excitation with ultraviolet light. Two-photon microscopy systems using pulsed femtosecond laser exposures provide high sensitivity with less phototoxicity, and thus may be used to monitor PAH in live cell systems. XS106 were observed to readily internalize DMBA immediately after exposure, with increasing accumulation evident as discrete intracellular foci over 1 hour, in all cells observed (Figure 2a, Supplementary Movie S1 online). LC isolated from murine skin, in contrast, showed an approximately 10 minute delay in the appearance of intracellular DMBA foci; yet, numbers of foci per cell accumulated with rapid kinetics to reach levels comparable to that seen in XS106 cells by 20 minutes after exposure (Figure 2a, Supplementary Movie S2 online). Individual foci size increased over time (Figure 2b) indicating intracellular concentration of DMBA. One hour post DMBA exposure, high-resolution z-stack confocal images of isolated LC and XS106 cells with surface membranes labeled with antibodies to MHC-II (Figure 2c-d, Supplementary Figure S1 online) revealed the internalized DMBA as numerous, variably-sized foci that were excluded from the nuclei. Consistent with the foci representing cytoplasmic collections into hydrophobic micro-droplets following trans-membrane diffusion, there was no evidence of endocytic vesicle formation or membrane-bound containment of the DMBA by either MHC-II (Figure 2c,d, Supplementary Figure S1 online) or PKH26 red fluorescent membrane tracking dye (Figure 2e). After a 1 hour exposure to DMBA, isolated LC that were transferred to fresh media

without DMBA showed persistent depots of internalized DMBA, even after 24 hours (Figure 2f, Supplementary Movie S3 online). Thus, LC have the capacity for rapid intracellular accumulation of DMBA. The delay in the appearance of DMBA foci within isolated LC (relative to that within XS106) suggests that normal LC may utilize an activated diffusion prior to the more passive diffusion, while the complete absence of MHC-II-containing membranes and PKH26 around the DMBA foci indicates that this internalization is not the result of endocytosis. Furthermore, the observed nuclear exclusion is consistent with cellular processes that may protect against LC's own genotoxicity.

Embryonic LC-precursors repopulate the skin of neonatal LC-deficient mice

Taken together, the observed characteristics of LC handling of DMBA (Figure 1,2) suggest LC enhancement of epidermal carcinogenesis by DMBA internalization, focal concentration, AhR-driven expression of metabolizing CYP1B1, and potential transfer of mutagenic metabolites to adjacent keratinocytes. Consistent with this, we previously demonstrated that DMBA applied to the skin resulted in higher rates of epidermal cell DNA-damage and increased tumor formation in LC-intact mice relative to LC-deficient mice (Modi *et al.*, 2012). To better elucidate the previously observed capacity of LC to facilitate epidermal cell genotoxicity and enhance tumor development, we developed a strategy for the efficient repopulation of LC within LC-deficient mice. Recently, it was identified that LC-progenitors first derive as an F4/80^{bright} macrophage-precursor population within the embryonic yolk sac, emerging around embryonic age (E) day 10 to seed the primitive skin directly, or to first expand within the E10–14 liver, prior to seeding and expanding in the embryonic skin (Schulz *et al.*, 2012; Hoeffel *et al.*, 2012). Therefore, we hypothesized that E10.5 yolk sac and E12.5 liver mononuclear cells when injected intraperitoneally into LC-deficient mice would seed the skin and expand to repopulate the LC compartment by adulthood, as we and others have demonstrated previously for skin repopulation of dendritic epidermal T cells (DETC) using E14–17 thymocytes (Havran and Allison, 1990; Payer *et al.*, 1991; Girardi *et al.*, 2002). In fact, both E10.5 yolk sac and E12.5 liver LC precursors were capable of repopulating the epidermis when transferred into newborn LC-deficient DTA, with the E12.5 liver showing slightly greater efficiency (Figure 3a). Notably, three weeks following transfer, LC were observed as circular expanding populations in the recipient epidermis (Figure 3b), and by 8 weeks eventually filled the epidermis of adult recipients (Supplementary Figure S2 online). These observations provide insight into the normal physiologic population of the epidermis by LC precursors present within embryonic yolk sac (Schulz *et al.*, 2012) and embryonic liver (Hoeffel *et al.*, 2012), and the "seed-soil" relationship of precursors that can expand over weeks after seeding the immature skin.

To examine the effect of recipient age at time of transfer on the ability of precursors to enter the epidermis and expand, E12.5 liver-derived LC-precursors were injected intraperitoneally into LC-deficient recipients ranging in age from <36 hours to 5 weeks, and the resulting epidermal LC populations analyzed and compared to age-matched normal controls. LC were re-established most efficiently when transferred into newborn recipients (Figure 3c) and display phenotypic (Figure 3d) and morphologic (Figure 3e) characteristics of normal LC. The requirement for neonatal skin, with marked decreasing efficiency of LC repopulation in recipients >36 hours old, is in contrast to our experience with repopulation of DETC where

E16 thymocyte precursors will repopulate adult epidermis provided the skin is in active hair growth at the time of transfer (Supplementary Table S1 online).

CYP1B1 expression by LC is required for maximal genotoxicity of adjacent keratinocytes and tumor development

Despite the fact that keratinocytes express the enzymes (CYP1A1, CYP1B1, and epoxide hydrolase) necessary to metabolize DMBA to its ultimate mutagenic form, DMBADE, we previously proposed that the higher ratio of CYP1A1:CYP1B1 within keratinocytes favors detoxification (Modi *et al.*, 2012). Given the capacity of LC to internalize and depot DMBA (Figure 1,2), and our previous demonstration of the capacity of LC to metabolize DMBA to its penultimate mutagenic form, DMBA-3,4-diol, we hypothesized that CYP1B1 expression within LC would be required for maximal genotoxicity of adjacent keratinocytes after epidermal exposure to DMBA. Thus, we repopulated LC-deficient mice with E12.5 liver LC-precursors from CYP1B1−/− mice (courtesy of F. Gonzalez; Buters *et al.*, 1999), that we first backcrossed to the FVB background by speed congenic breeding, and compared them to LC-deficient mice repopulated with precursors from wild-type (w.t., CYP1B1-competent) FVB mice. LC repopulation levels and LC surface phenotype and morphology was equivalent in DTA recipients of w.t. or CYP1B1−/− LC precursors (Figure 3c–e).

Phosphorylated (γ)H2Ax is recruited to dsDNA breaks and DNA-PAH adducts, and is therefore a non-specific but sensitive indicator of DNA damage, including that as a result of DMBA exposure (Modi *et al.*, 2012). 24 hours after a single application of DMBA, LC-deficient mice repopulated with LC-precursors from wild-type mice showed levels of γH2Ax comparable to that of wild-type mice (Figure 4a,b). Thus, repopulation of LC by intraperitoneal injection of embryonic liver isolated LC-precursors into neonatal recipients results by adulthood in functionally competent LC, capable of facilitating keratinocyte genotoxicity after DMBA exposure. In contrast, LC-deficient mice repopulated with LC-precursors from syngeneic CYP1B1−/− mice showed significantly reduced levels of γH2Ax relative to LC-intact controls, but which were statistically distinguishable from that of mice devoid of all LC (Figure 4a,b). Therefore, CYP1B1 expression specifically within LC contributes substantially to neighboring keratinocyte DNA damage following DMBA exposure, even though this DMBA metabolizing enzyme is present in the surrounding cells. In addition, the observation that DTA mice repopulated with CYP1B1−/− LC had increased DNA damage compared to mice devoid of all LC indicates that LC also participate in CYP1B1-independent events that facilitate damage of surrounding cells. Within each of the DMBA-exposed groups, only ~1% of LC showed γH2AX staining indicative of DNA damage, while LC density 24 hours post-DMBA exposure was not distinguishable from that of untreated mice (Supplementary Table S2 online). This, together with the observed lack of nuclear DMBA fluorescence within LC (Figure 2d), suggests LC may possess mechanisms to guard against their own genotoxicity while contributing to adjacent keratinocyte damage.

When groups of LC repopulated and control mice were followed for tumor development using the standard DMBA-TPA model, LC-deficient mice repopulated with LC-precursors from wild-type embryos were again similar to normal FVB (LC-intact) mice (Figure 5a–c), and the level of LC reconstitution measured at 8 weeks, i.e. immediately prior to initiation

with DMBA, was directly correlated with the extent of tumor development (R=0.7528; P=0.0155, data not shown). In contrast, LC-deficient mice repopulated with CYP1B1-deficient LC precursors were indistinguishable by tumor area/mouse (Figure 5a) or tumor area/tumor-bearing mouse (Supplementary Table S3 online) from LC-deficient control DTA mice through 12 weeks of tumor promotion, and showed markedly reduced tumor susceptibility relative to LC-deficient mice repopulated with w.t. LC precursors and NLC (w.t.) controls (Figure 5a–c).

However, tumors in DTA mice repopulated with CYP1B1−/− LC did arise earlier than in DTA controls (Figure 5c). This suggested that LC exerted CYP1B1-independent effects on tumor promotion. Therefore we continued to follow co-caged cohorts of DTA and DTA repopulated with CYP1B1−/− LC. Notably, tumor growth was observed to statistically increase in CYP1B1-deficient LC-repopulated mice, relative to LC-deficient controls at 14 weeks, further suggesting a CYP1B1-independent tumor-promoting role for LC (Figure 5d,e). Consistent with this, independent studies in DMBA-naïve mice showed increased epidermal hyperplasia in LC-intact skin relative to LC-deficient skin after repeated exposure to TPA alone (Figure 5f) and increased ear thickness 48 hours following a single application of TPA (Figure 5g). Each of these results suggests LC influence the response to epidermal perturbation, directly or indirectly promoting eventual keratinocyte proliferation that is fundamental to tumor promotion.

Collectively, our data reveal multiple distinct roles for LC in chemical carcinogenesis: (1) morphologic and structural features that support efficient PAH internalization and depot within LC, (2) metabolism to mutagenic metabolites that are specifically dependent on LC expression of CYP1B1, and (3) CYP1B1-independent contributions to DNA-damage within adjacent keratinocytes and to tumor promotion. The contributions of immune cells to tumor growth have been previously characterized to include the activities of tumor-associated macrophages, tumor-promoting T cells (Kwong *et al.*, 2010), and T-regulatory cells that may increase oxidative stress, provide growth factors, and suppress anti-tumor immunity to facilitate tumor immune evasion and growth. We have extended these untoward effects of immune cells under the concept of cooperative carcinogenesis to emphasize that immune cells may be fundamental to the full spectrum of initiation and promotion.

Major lines of epidemiologic and experimental study have linked mutagenic PAHs to cancer within a variety of tissues (e.g. skin, lung, gastrointestinal, bladder, breast) (Boffetta *et al.*, 1997; Armstrong *et al.*, 2004). In addition, a role for mutagenic PAHs in cutaneous carcinogenesis, including their potentiation of ultraviolet (UV) radiation, has been implicated by several lines of laboratory investigation. Purified particles of air pollution applied to the skin of mice can serve as an initiator of cutaneous carcinogenesis, and this is dependent on the expression of the intracellular aryl hydrocarbon receptor (AhR) for PAHs (Matsumoto *et al.*, 2007). Initiation by topical application of mutagenic benzo[*a*]pyrene followed by exposure to UV radiation synergistically provoke skin tumor formation in mice (Burke *et al.*, 2009). Furthermore, chronic exposure of mice to both inhalation of PAH-containing tobacco smoke and UV radiation induces the outgrowth of cutaneous SCC at a much greater rate than either agent alone (Pavlou *et al.*, 2009). A single application of the PAH 7,12-dimethylbenz[*a*]anthracene (DMBA) prior to UV radiation of human skin

xenografts markedly increases the development of actinic keratoses and SCC, relative to the same dose of UV alone (Berking *et al.*, 2002). Thus, although UV radiation is well established as a genotoxic agent associated with human skin cancer risk, these studies collectively reveal the potential of chemical mutagenesis by PAHs as an underappreciated co-factor in the induction of human cutaneous malignancy.

Squamous cell carcinomas comprise the most common human solid tumor malignancy including those of skin, gastrointestinal, genitourinary, breast, and lung origins. They derive, by definition, from continuously regenerating epithelial cells that encompass large surface areas at the interface with the environment, where they may be exposed to myriad environmental compounds, including mutagenic PAHs. In addition to direct contact with exogenous agents of DNA-damaging potential, systemic absorption of such mutagens through the epithelium (e.g. via smoking, industrial exposures, diets high in grilled meats) can lead to more global tissues exposures. Since CYP1B1 has also been shown metabolize the carcinogenic PAH benzo[*a*]pyrene (BAP) to its mutagenic intermediate (Shimada *et al.*, 1999), and an elevated CYP1B1:CYP1A1 ratio has been reported in human monocyte/macrophage subsets (Baron *et al.*, 1998), it is conceivable that a spectrum of benz[*a*]athracene and BaP related compounds present in the environment might be predicted to undergo similar handling and activation within the skin and other tissues.

Moreover, it is also possible that differential cellular expression of metabolizing enzymes other than CYP1B1 may also contribute to carcinogenesis. For example, LC also preferentially expresses CYP2E1 (Saeki *et al.*, 2002) which has the capacity to activate several carcinogens including benzene (Valentine *et al*., 1996) and azoxymethane (Sohn *et al.*, 2001). Thus, while we believe our findings definitively demonstrate that LC expression of CYP1B1 is fundamental to DMBA mutagenesis of neighboring keratinocytes, further investigation is warranted to fully appreciate its potential generalizability to other dendritic cell populations, other metabolizing enzymes, and other epithelial and non-epithelial tissues.

The roles (beyond antigen presentation) of Langerhans cells in cutaneous biology have been expanded to also include their potential for immune regulation (Kaplan *et al.*, 2005). Since *initiation* effects of LC are independent of adaptive immunity (that is, occurring in the absence of all T cells; Modi *et al.*, 2012; Strid *et al.*, 2008), it is unlikely that T cell mediated regulation plays a significant role in this stage of chemical carcinogenesis. In contrast, the previously described tumor-promoting αβ T cells and anti-tumor γδ T cells (Kwong *et al.*, 2010; Roberts *et al.*, 2007; Girardi *et al.*, 2003; Girardi *et al.*, 2001) raise the possibility that these components of adaptive immunity may interact with LC to, in aggregate, contribute to tumor *promotion*. In this regard, application of higher doses of DMBA (or ultraviolet light) to mouse skin results in depletion of LC largely due to migration to draining lymph nodes, and percutaneous immunization in such mice shows blunted antigen-specific responses that might include anti-tumor effects (Qu *et al.*, 1997; Ragg *et al*., 1995). Thus, while we have herein provided additional insight into mechanisms by which LC influence chemical carcinogenesis, further studies are necessary to more clearly delineate the complexity of interactions between LC and other immune cells in regulating tumor promotion.

Materials and Methods

Animals and Housing

Mice were maintained under specific pathogen-free conditions in a facility accredited by the Association for Assessment of Laboratory Animal Care with food and water provided *ad libitum*. The Yale Animal Care and Use Committee approved all *in vivo* studies. FVB/N mice were purchased from The Jackson Laboratory. FVB/N LC deficient (DTA) mice were generated with a bacterial artificial chromosome-based transgene containing human Langerin modified to drive expression of diphtheria toxin subunit A from an internal ribosome entry site inserted in the 3′ untranslated region of the langerin gene (Kaplan *et al.*, 2005). *Cyp1b1*−/− mice were kindly provided by F. Gonzalez (NCI, Bethesda, MD) and backcrossed onto the FVB background via speed congenic methodology (testing provided by IDEXX RADIL, Columbia, MO) for 6 generations.

DMBA fluorescence

The LC-like cell line XS106 was kindly provided by A. Takashima (U of Toledo, OH) and cultured as previously described (Modi *et al.*, 2012). Epidermal cell suspensions were prepared as previously described (Strid *et al.*, 2008) and LC enriched using either MHC II- or CD45-magnetic beads (Miltenyi Biotec) followed by staining with PE- or FITC-MHC II (eBioscience) and MoFlo (Dako) cell sorting to obtain 98% purity. XS106 or purified LC were cultured overnight in 35 mm glass bottom culture dishes (MatTek Corp) in phenol red-free RPMI 1640 (Invitrogen) containing 10% FBS, 10 mM Hepes, 1% non-essential amino acids, 2 mM L-glutamine, 1mM sodium pyruvate, 0.05 mM β-mercaptoethanol, and antibiotics before use in DMBA fluorescence monitoring. DMBA (Sigma; 64μM) was added after images of untreated cells were collected. Imaging was performed using a Zeiss 710 Duo NLO/Multiphoton microscope running Zen 2010 software and equipped with a Spectra-Physics MaiTai titanium:sapphire laser for two-photon excitation, and an enclosed CO_2 incubator (37°C). DMBA fluorescence was collected from 400–490nm (peak 440nm). In some experiments FITC or PE-MHC II (eBioscience) antibody was added (0.25 μg/ml) to permit LC cell membrane visualization. XS106 was labeled with CyTRAK Orange (5 μM, eBioscience) or membrane dye PKH26 (Sigma) according to manufacturer's instructions and exposed to DMBA (16 μM) for 1 hour before z-stacked images were obtained. Live time series images were taken every 2 or 2.5 minutes over 1 hour. Individual cells and contained DMBA foci were identified and quantitated using ImageJ v1.47 (NIH).

Confocal microscopy

Epidermal sheets were prepared following a 2 hour 37°C incubation in 20 mM EDTA (for LC morphology post-DMBA application and LC and DETC visualization in repopulated mice) or a 20 minute 37°C incubation in 0.5 M ammonium thiocyanate (for γH2AX analysis), fixed 20 minutes in ice-cold acetone, rehydrated in PBS, blocked with 2% BSA and stained using the following antibodies: anti-CD207 (1.5 μg/ml, RMUL.2, eBioscience) + Alexa488- or Cy3-Donkey-anti-rat IgG (Jackson Immunoresearch), anti-TCRγδ (1.5 μg/ml, GL3, Becton Dickinson) + Cy3-goat anti-hamster IgG (Jackson Immunoresearch), anti-γH2AX (1 μg/ml, JBW30, Millipore) + Alexa568-Goat-anti-mouse IgG (Invitrogen), FITC-MHC II (1.6 μg/ml, M5/114.15.2, Biolegend). Samples were examined using a Zeiss

510Meta confocal microscope. Analysis of γH2AX+ cells was performed as previously described (Modi *et al.*, 2012). Briefly, 35 nmoles DMBA was applied to the dorsal surface of each ear and 24 hours later epidermal sheets prepared, stained and z-stacked images of 10 fields/sheet (2 sheets/mouse) collected in a set pattern in 2 mm intervals. ImageJ (NIH) particle analyzer software was used to identify and quantitate γH2AX+ cells. For analysis of LC morphology 24 hours post DMBA application, images collected as described above were analyzed using Volocity 6.2 (Perkin Elmer) for LC identification and measurement of shape factor (circularity on a scale of 0–1 with 1=circle). The mean and distribution of shape factor measurements was calculated using Prism 6.0 (GraphPad).

Gene expression analysis

RNA was isolated from XS106 cells using RNeasy Micro kit (Qiagen) and transcribed using High-Capacity cDNA Reverse Transcription kit (ABI). Real-time quantitative RT-PCR (ABI 7500, SDS 2.0 software) was performed using Taqman assays and Taqman Gene Expression Mastermix (ABI). Obtained Ct values were normalized to β-actin and expression differences to untreated samples calculated using $RQ=2^{-\Delta\Delta Ct}$.

Flow cytometric analysis

To examine LC phenotype following DMBA exposure, epidermal cells suspensions were prepared as previously described (Strid *et al.*, 2008) from dorsal bodywall of FVB/N mice that had been clipped and treated with depilatory cream 5 days earlier and treated with vehicle (acetone) or DMBA (400 nmoles) 24 hours before harvest. After blocking FcR (CD16/32), cells were stained with PerCPCy5.5-CD45, PE-MHC II, APC-CD86 (all from eBioscience) and Alexa488-CD207 (Imgenex) and data collected using FACSCalibur (Becton Dickinson) and analyzed with FlowJo (TreeStar). To assess LC repopulation levels, epidermal cell suspensions were prepared from either ear punch biopsy (prior to DMBA application in carcinogenesis studies) or from untreated bodywall skin. Epidermal cells from LC-intact (NLC) and LC-deficient (DTA) as well as those from each repopulated mouse were blocked (CD16/32) and stained with APC-CD45 + PE-MHC II + Alexa488-CD207. In each experiment the average percentage of CD45+MHCII+CD207+ epidermal cells in NLC controls was calculated and the percent LC repopulation of each individual yolk sac or liver recipient determined by comparison.

LC repopulation

E10.5 yolk sac or E12.5 liver was isolated from donor embryos. Yolk sac was digested as described (Morgan *et al.*, 2008) by incubation in 0.25% collagenase in PBS containing 20% FBS for 40–60 minutes at 37°C. Liver was dissociated by gentle pipetting. Cells were washed once in PBS + 10% FBS and resuspended in PBS at 4 donor equivalents per 30 μl. Newborn LC-deficient recipients received 30 μl donor cells by intraperitoneal injection. The level of LC repopulation was assessed by flow cytometric analysis.

Two-stage chemical carcinogenesis

As previously described (Modi *et al.*, 2012) at age 7 weeks, dorsal bodywall hair was removed by shaving with electric clippers followed by application of depilatory cream. One

week later carcinogenesis was initiated by application of DMBA (400 nmoles, Sigma) in acetone. One week following initiation, twice-weekly applications of TPA (20 nmoles, Sigma) in ethanol began. Tumors were counted, measured, and scored weekly as clinically apparent papillomas (i.e. well-demarcated, symmetrical, pedunculated, or dome-shaped papules, without erosion or ulceration) or clinically apparent carcinomas (poorly demarcated, asymmetrical, non-pedunculated, or dome-shaped papules with erosion or ulceration) by an observer blinded to the experimental groups, as previously described (Girardi *et al.*, 2003). After 12 weeks of promotion, tumor burden was a humane concern for NLC and DTA+w.t. LC groups, therefore only co-caged cohorts of DTA and DTA +CYP1B1−/− LC groups were carried through 14 weeks. At the conclusion of experiments, representative tumors were excised, fixed and embedded for hematoxylin and eosin staining and were examined by a certified dermatopathologist (C.K.) for histologic confirmation. The terms “tumor area” and “tumor number” are used to refer to all tumors present (papillomas + carcinomas).

Irritant responses

For analysis of epidermal hyperplasia, TPA (20 nmoles) in ethanol was applied to dorsal bodywall skin twice weekly for 4 weeks, then formalin fixed paraffin embedded samples prepared, stained with hematoxylin and eosin and examined using an Olympus BH10 microscope equipped with an optical micrometer. Minimal epidermal thickness was measured from the basal to the granular layer of the epidermis in 12 fields/section in 4 samples/mouse. Ear thickness following a single application of TPA (0.5 nmoles to each side of each ear) was measured using an engineer’s micrometer (Mitutoyo 7301). Measurements were made by an observer blind to the experimental groups.

Statistical analysis

One-tailed Student’s *t* test for unpaired data was used to determine the statistical significance of difference between experimental groups in all cases except Figure 1A, 1B, 1D, 5A and 5C, with significance at $P < 0.05$. Curves in Kaplan-Meier plots (Figure 5C) were compared using the log-rank test. Changes in tumor area or gene expression over time (Figure 1A, 1B, 5A) were compared using repeated measures ANOVA with appropriate correction for multiple time point and multiple group comparisons (Tukey’s correction for Figure 5A, Sidak’s correction for Figure 1A and 1B). Frequency distributions (Figure 1D) were compared with the nonparametric Kolmogorov-Smirnov test. All statistical analyses were performed with GraphPad Prism 6.0 software.

Supplementary Material

Refer to Web version on PubMed Central for supplementary material.

Acknowledgments

Funding for this work was provided by the NIH grant R01CA102703 (to M.G.) and the Novartis Foundation for Medical-Biological Research (to C.B). We thank F. Geissman (KCL) and F. Ginhoux (A*STAR) for protocol advice, A. Takashima (U Toledo) for XS106 cells, and F. Gonzalez (NCI) for *Cyp1b1*−/− mice.

Abbreviations

AhR	aryl hydrocarbon receptor
DMBA	dimethylbenz[*a*]anthracene
DTA	hHuLangerin-DTA transgenic Langerhans cell deficient mouse
E	embryonic day
LC	Langerhans cell
PAH	polyaromatic hydrocarbon
SCC	squamous cell carcinoma
TPA	12-O-tetradecanoylphorbol-13-acetate

References

Armstrong B, Hutchinson E, Unwin J, et al. Lung Cancer Risk after Exposure to Polycyclic Aromatic Hydrocarbons: A Review and Meta-Analysis. Environ Health Perspect. 2004; 112:970–978. [PubMed: 15198916]

ATSDR/CDC. Agency for Toxic Substances and Disease Registry. Division of Toxicology and Human Health Sciences; Atlanta, GA: 2011. http://www.atsdr.cdc.gov/substances/toxsubstance.asp?toxid=25

Baron J, Zwadlo-Klarwasser G, Jugert F, et al. Cytochrome P450 1B1: A major P450 isoenzyme in human blood monocytes and macrophage subsets. Biochem Pharmacol. 1998; 56:1105–10. [PubMed: 9802319]

Berking C, Takemoto R, Binder RL, et al. Photocarcinogenesis in human adult skin grafts. Carcinogenesis. 2002; 23:181–7. [PubMed: 11756239]

Boffetta P, Jourenkova N, Gustavsson P. Cancer risk from occupational and environmental exposure to polycyclic aromatic hydrocarbons. Cancer Causes Control. 1997; 8:444–72. [PubMed: 9498904]

Burke KE, Wei H. Synergistic damage by UVA radiation and pollutants. Toxicol Ind Health. 2009; 25:219–24. [PubMed: 19651790]

Buters JT, Sakai S, Richter T, et al. Cytochrome P450 CYP1B1 determines susceptibility to 7, 12-dimethylbenz[*a*]anthracene-induced lymphomas. Proc Natl Acad Sci U S A. 1999; 96:1977–82. [PubMed: 10051580]

Girardi M, Oppenheim DE, Steele CR, et al. Regulation of cutaneous malignancy by gammadelta T cells. Science. 2001; 294:605–609. [PubMed: 11567106]

Girardi M, Lewis J, Glusac E, et al. Resident skin-specific γδ T cells provide local, nonredundant regulation of cutaneous inflammation. J Exp Med. 2002; 195:855–867. [PubMed: 11927630]

Girardi M, Glusac E, Filler RB, et al. The distinct contributions of murine T cell receptor (TCR) gammadelta+ and TCRalphabeta+ T cells to different stages of chemically induced skin cancer. J Exp Med. 2003; 198:747–755. [PubMed: 12953094]

Havran WL, Allison JP. Origin of Thy-1+ dendritic epidermal cells of adult mice from fetal thymic precursors. Nature. 1990; 344:68–70. [PubMed: 1968230]

Hoeffel G, Wang Y, Greter M, et al. Adult Langerhans cells derive predominantly from embryonic fetal liver monocytes with a minor contribution of yolk sac-derived macrophages. J Exp Med. 2012; 209:1167–81. [PubMed: 22565823]

Ilchmann A, Krause M, Heilmann M, et al. Impact of culture medium on maturation of bone marrow-derived muring dendritic cells via the aryl hydrocarbon receptor. Mol Immunol. 2012; 51:42–50. [PubMed: 22377453]

Kaplan DH, Jenison MC, Saeland S, et al. Epidermal langerhans cell-deficient mice develop enhanced contact hypersensitivity. Immunity. 2005; 23:611–20. [PubMed: 16356859]

Kwong BY, Roberts SJ, Silberzahn T, et al. Molecular analysis of tumor-promoting CD8+ T cells in two-stage cutaneous chemical carcinogenesis. J Invest Dermatol. 2010; 130:1726–36. [PubMed: 19924136]

Leonardi-Bee J, Ellison T, Bath-Hextall F. Smoking and the risk of nonmelanoma skin cancer: systematic review and meta-analysis. Arch Dermatol. 2012; 148:939–46. [PubMed: 22711192]

Matsumoto Y, Ide F, Kishi R, et al. Aryl hydrocarbon receptor plays a significant role in mediating airborne particulate-induced carcinogenesis in mice. Environ Sci Technol. 2007; 41:3775–80. [PubMed: 17547212]

Modi BG, Neustadter J, Binda E, et al. Langerhans cells facilitate epithelial DNA damage and squamous cell carcinoma. Science. 2012; 335:104–8. [PubMed: 22223807]

Morgan K, Kharas M, Dzierzak E, et al. Isolation of early hematopoietic stem cells from murine yolk sac and AGM. J Vis Exp. 2008; 16 pii:789. 10.3791/789

Pavlou P, Rallis M, Deliconstantinos G, et al. In-vivo data on the influence of tobacco smoke and UV light on murine skin. Toxicol Ind Health. 2009; 25:231–9. [PubMed: 19651792]

Payer A, Elbe A, Stingl G. Circulating CD3+/T cell receptor Vγ3+ fetal murine thymocytes home to the skin and give rise to proliferating dendritic epidermal T cells. J Immunol. 1991; 146:2536–2543. [PubMed: 1826696]

Qu M, Muller HK, Woods GM. Chemical carcinogens and antigens contribute to cutaneous tumor promotion by depleting epidermal Langerhans cells. Carcinogenesis. 1997; 18:1277–1279. [PubMed: 9214614]

Ragg S, Dandie G, Woods GM, et al. Dendritic cells migrating from carcinogen-treated skin have reduced antigen-presenting function. Adv Exp Med Biol. 1995; 378:237–241. [PubMed: 8526064]

Roberts SJ, Ng By, Filler RB, et al. Characterizing tumor-promoting T cells in chemically induced cutaneous carcinogenesis. Proc Natl Acad Sci USA. 2007; 104:6770–6775. [PubMed: 17412837]

Schulz C, Gomez Perdiguero E, et al. A lineage of myeloid cells independent of Myb and hematopoietic stem cells. Science. 2012; 336:86–90. [PubMed: 22442384]

Shimada T, Gillam E, Oda Y, et al. Metabolism of benzo[*a*]pyrene to *trans*-7,8-dihydroxy-7,8-dihydrobenzo[*a*]pyrene by recombinant human cytochrome P450 1B1 and purified liver epoxide hydrolase. Chem Res Toxicol. 1999; 12:623–629. [PubMed: 10409402]

Simones T, Shepherd D. Consequences of AhR Activation in Steady-State Dendritic Cells. Toxicol Sci. 2011; 119:293–307. [PubMed: 21097750]

Strid J, Roberts S, Filler R, et al. Acute upregulation of an NKG2D ligand promotes rapid reorganization of a local immune compartment with pleiotropic effects on carcinogenesis. Nat Immunol. 2008; 9:146–154. [PubMed: 18176566]

Werley MS, Freelin SA, Wrenn SE, et al. Smoke chemistry, in vitro and in vivo toxicology evaluations of the electrically heated cigarette smoking system series K. Regul Toxicol Pharmacol. 2008; 52:122–39. [PubMed: 18590791]

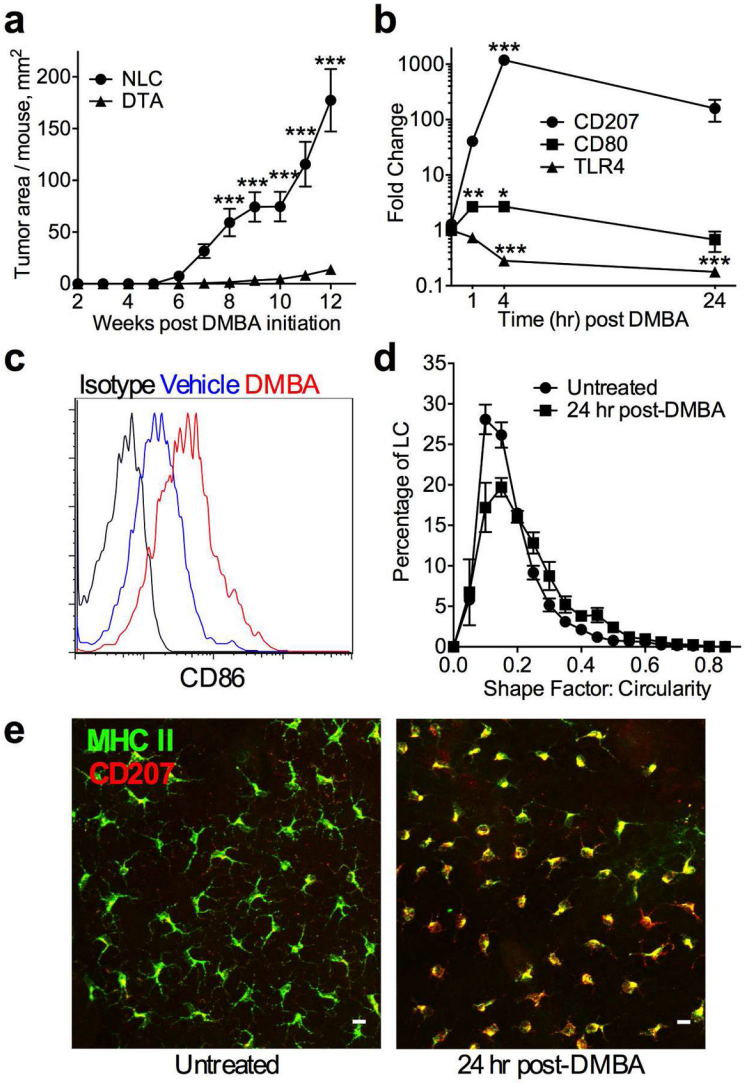

Figure 1. LC facilitate DMBA-initiated cutaneous carcinogenesis and display phenotypic and morphologic changes in response to DMBA exposure

(**a**)Carcinogenesis initiated in LC-intact (NLC) and LC-deficient (DTA) mice by application of DMBA (400 nmoles) followed by twice weekly TPA (20 nmoles, n=13–15 mice/group, *** $P \leq 0.001$). (**b**) XS106 was treated with 64μM DMBA and changes in gene expression monitored by quantitative real-time PCR, * $P < 0.05$, ** $P \leq 0.01$, *** $P \leq 0.001$. (**c**) FVB/N dorsal bodywall was treated with vehicle (acetone) or 400 nmoles DMBA, epidermal cell suspensions prepared 24 hours later and stained for flow cytometric analysis. Population shown is gated on CD45+ CD207+ cells. LC from untreated (not shown) and vehicle treated mice had similar CD86 expression (ΔMFI = 20.4 vs 17.3; P = n.s.). LC CD86 expression increased following DMBA treatment (ΔMFI = 54.4, P = 0.0013 vs vehicle, n=3 mice/group). (**d,e**) FVB/N dorsal ears were treated with 35 nmoles DMBA, epidermal sheets prepared 24 hours later and stained with CD207 (red) + MHC II (green). LC were identified and their shape factor (circularity ranging from 0–1, circle = 1. Mean ± SE untreated 0.1825

± 0.0019, DMBA treated 0.2254 ± 0.0028, $P < 0.0001$) measured using Volocity 6.2, n=3 mice/group. Scalebar = 10μm.

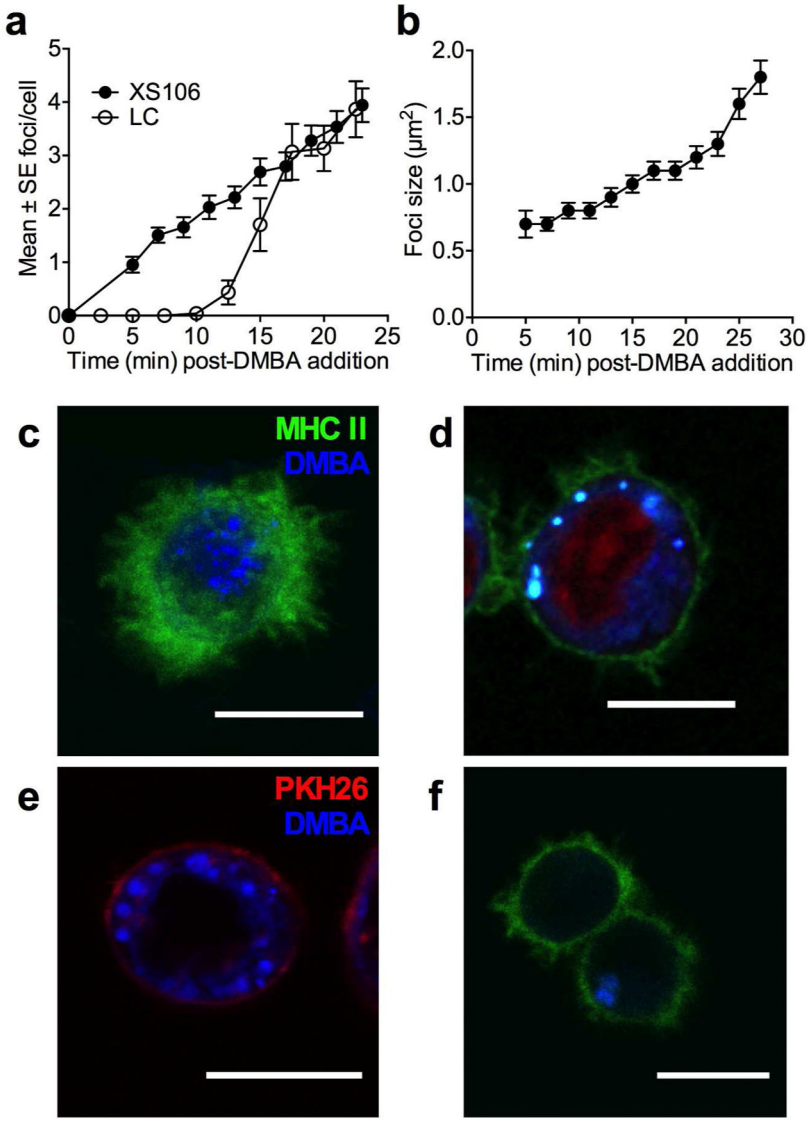

Figure 2. LC rapidly internalize DMBA as intracellular foci

(**a**) DMBA (64μM) was added to the LC cell line, XS106, or isolated LC and DMBA fluorescence followed using two-photon microscopy and time-series images collected every 2 minutes (XS106, Supplementary Movie S1 online) or 2.5 minutes (LC, Supplementary Movie S2 online) over 1 hour. DMBA foci within individual cells (n=148 XS106, n=81 LC) were identified and quantitated over the first 25 minutes using ImageJ. (**b**) Individual foci identified within XS106 during the first 10 minutes of DMBA exposure were measured and followed using ImageJ. (**c**) Compressed z-stack of isolated LC (FITC-MHC II, green) following 1 hour DMBA (blue) exposure. Single slices of z-stack (Supplementary Figure S1 online) suggest nuclear exclusion of DMBA foci. (**d**) XS106 cells were labeled with FITC-MHC II (green) and the nuclear dye CyTRAK Orange (red) then exposed to DMBA (blue) for 1 hour. DMBA foci were excluded from the nucleus. (**e**) XS106 were labeled with the membrane dye PKH26 (red) then exposed to DMBA (blue) for 1 hour. (**f**) Isolated LC were exposed to DMBA for 1 hour, then washed and cultured for an additional 23 hours in the

absence of DMBA (Supplementary Movie S3 online). At this time, 42% of LC retained at least 1 DMBA focus, exemplified in the single slice of the z-stack shown.

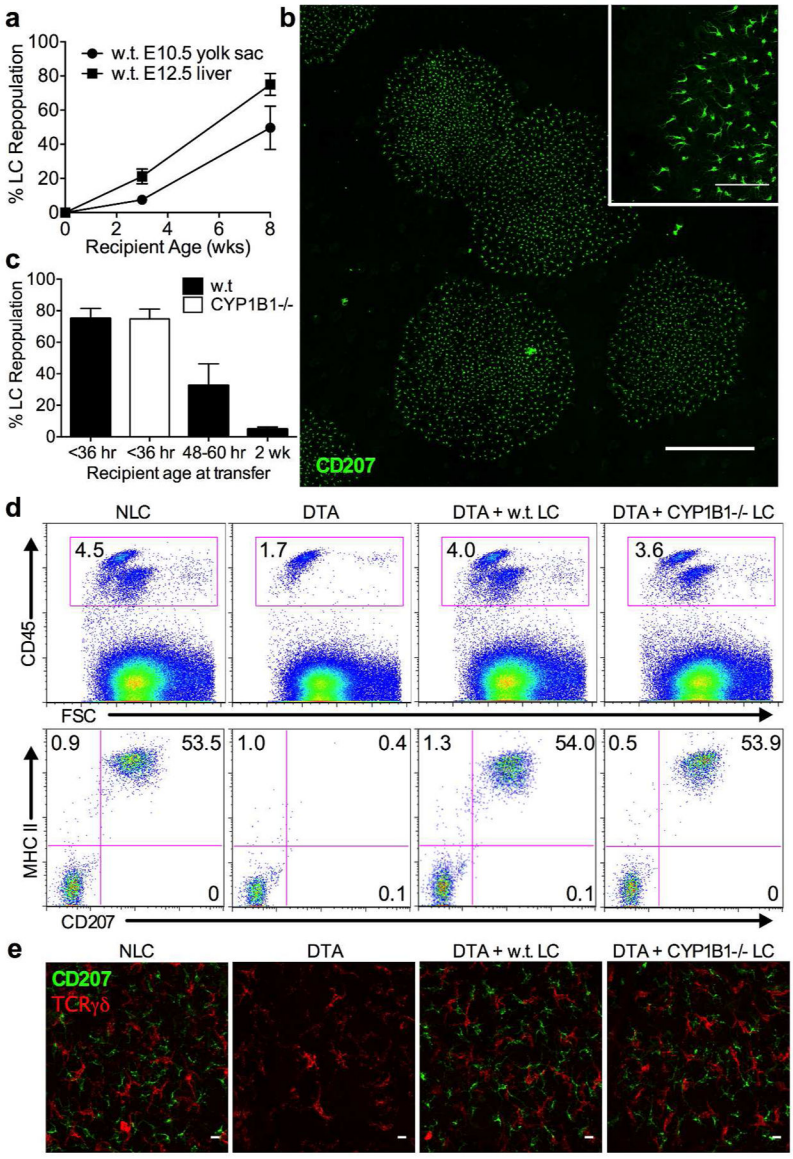

Figure 3. Embryonically derived LC-precursors repopulate LC-deficient DTA mice

(**a**) Cell suspensions prepared from w.t. E10.5 yolk sac or E12.5 liver were injected i.p. into newborn LC-deficient DTA recipients. Three or eight weeks later, flow cytometric analysis of epidermal cell suspensions prepared from recipients as well as NLC and DTA controls were used to determine the extent of LC repopulation. (**b**) Immunofluorescent staining of an epidermal sheet prepared from a DTA recipient 3 weeks following E12.5 liver transfer show expanding groups of LC (CD207, green). Scalebar = 500 μm. Inset scalebar = 100 μm. (**c**) E12.5 liver suspensions prepared from w.t. or CYP1B1−/− donors were injected i.p. into recipients of indicated ages. Epidermal cell suspensions prepared 8 weeks later and analyzed by flow cytometry show decreasing LC repopulation with increasing recipient age at time of transfer. No repopulation was detectable when recipients were 5 weeks old at transfer. (**d**) Flow cytometric analysis of epidermal cell suspensions prepared from bodywall skin of 8 week old NLC, DTA and DTA recipients of E12.5 liver. Upper panels are gated on total

epidermal cells; lower panels are gated on CD45+ cells. (**e**) Epidermal sheets prepared from bodywall skin 8 weeks following E12.5 liver transfer show typical LC (CD207, green) and DETC (TCRγδ, red) density and morphology when examined by confocal microscopy. Scalebar = 10 μm.

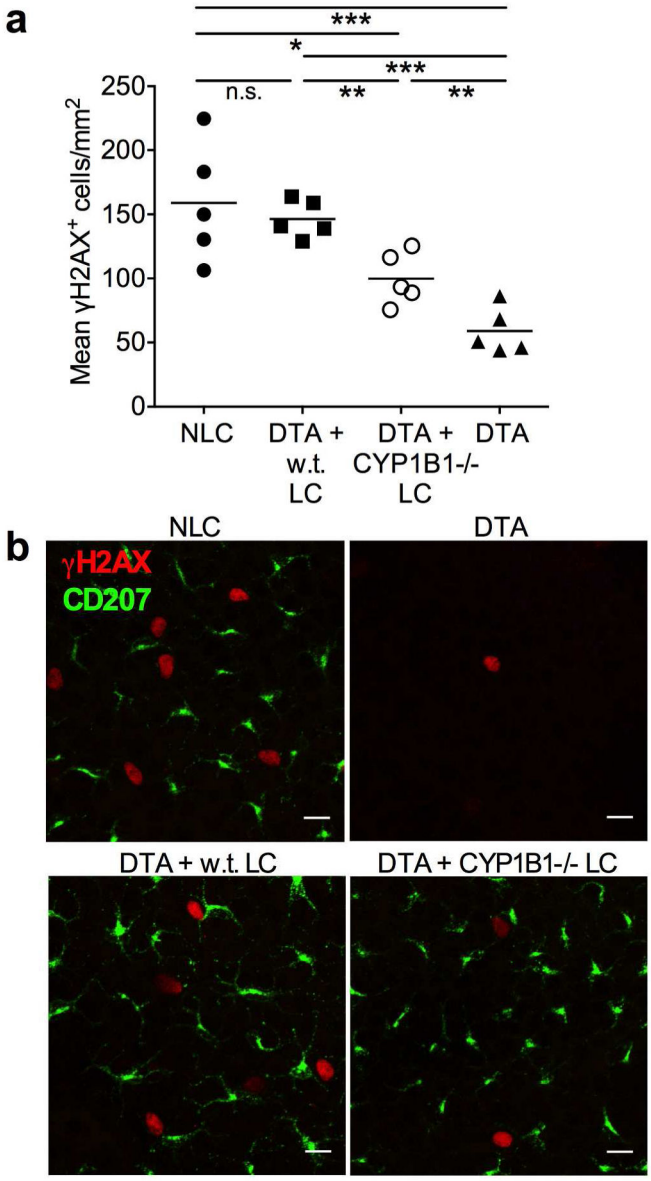

Figure 4. LC expression of CYP1B1 is necessary for optimal DMBA-induced DNA damage

(**a**) Ears of NLC and DTA controls as well as DTA repopulated with either w.t. or CYP1B1−/− LC were treated with 35 nmoles DMBA. 24 hours post-treatment epidermal sheets were prepared for γH2AX+ cell enumeration. Each dot represents one mouse. *P < 0.05, **P ≤ 0.01, ***P ≤ 0.001. (**b**) Representative confocal images from (a) show LC (CD207, green) and nuclei containing DNA damage (γH2AX, red). Scalebar = 10μm.

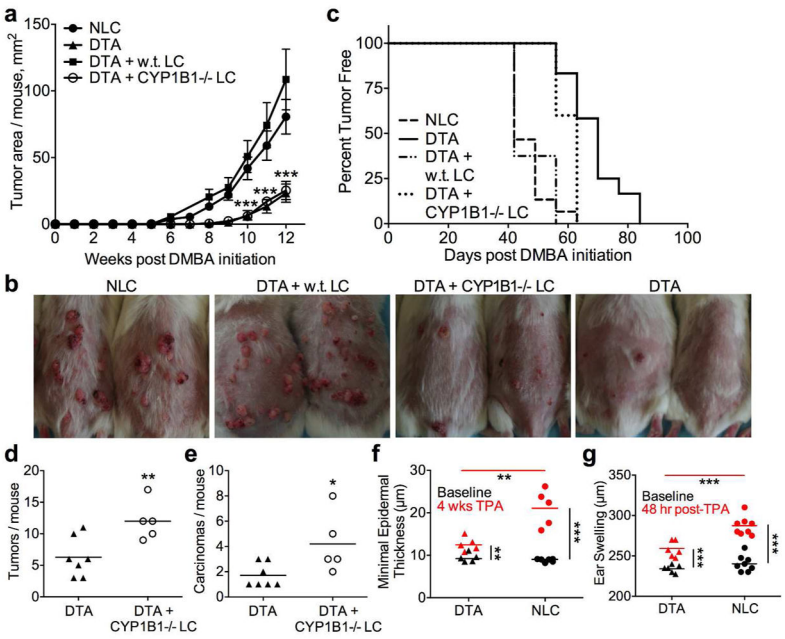

Figure 5. LC expression of CYP1B1 is required for optimal cutaneous chemical carcinogenesis

(**a**) Chemical carcinogenesis was initiated in NLC and DTA controls as well as DTA repopulated with either w.t. or CYP1B1−/− LC using 400 nmoles DMBA followed by twice weekly TPA promotion (20 nmoles); ***P < 0.001 DTA+CYP1B1−/− LC vs DTA+w.t. LC and vs NLC; and P < 0.001 for DTA vs DTA+w.t. LC and vs NLC. N = 5–15 mice/group for panels a–c. (**b**) Representative images from (a) taken 12 weeks following initiation. (**c**) Percentage of tumor-free mice over time depicted in Kaplan-Meier plot. P < 0.05 for DTA vs DTA+CYP1B1−/− LC, P ≤ 0.01 for DTA+CYP1B1−/− LC vs DTA+w.t. LC and vs NLC, P < 0.0001 for DTA vs NLC and vs DTA+w.t.LC. (**d,e**) 14 weeks post initiation, DTA repopulated with CYP1B1−/− LC have more total tumors (**d**) and carcinomas (**e**) than LC-deficient DTA; n=7 DTA, 5 DTA+CYP1B1−/−LC. (**f**) Epidermal hyperplasia, as measured by minimal epidermal thickness, in response to repeated TPA application (4 weeks) is greater in the presence of LC; n=5 DTA, 5 NLC. (**g**) Ear thickness 48 hours after a single TPA application is greater in the presence of LC; n=6 DTA, 8 NLC. Baseline ear thickness (g) and minimal epidermal thickness (f) are not different in DTA vs NLC. *P <0.05, **P ≤ 0.01, ***P ≤ 0.001. Each dot represents one mouse in panels d–g.